



ELSEVIER

International Journal of Solids and Structures xxx (2004) xxx–xxx

INTERNATIONAL JOURNAL OF  
**SOLIDS and  
STRUCTURES**

www.elsevier.com/locate/ijsolstr

## The influence of a weld-induced axi-symmetric imperfection on the buckling of a medium-length silo under wind loading

Martin Pircher \*

*Centre for Construction Technology and Research, Kingswood Campus, Bldg X, University of Western Sydney,  
Locked Bag 1797, Penrith South DC, NSW 1797, Australia*

Received 7 January 2004; received in revised form 1 May 2004

### Abstract

For particular geometrical constellations of thin-walled cylindrical structures under wind-loading, a peculiar stability failure mode has been observed. This failure mode is characterised by the occurrence of multiple horizontal ripple-like buckles in an area around the upper half of the windward meridian. A recent case study of a cylinder undergoing this type of buckling revealed the strong influence of localised axi-symmetric imperfections on this particular buckling behaviour. For the present paper a detailed investigation into the nature of this influence of such imperfections on the buckling behaviour under wind loading has been performed using finite elements models. A cylinder with a geometry that displayed the particular buckling pattern in question was considered for this study. The parameters describing the nature of the axi-symmetric weld imperfection were varied and their influence on the buckling of these cylinders was studied in detail. The present study draws from insights gained from similar studies for cylinders under axial loading. Many similarities between the two loading cases can be observed and the influence of weld-induced imperfections on the buckling under the two loading types were compared for this paper.

© 2004 Published by Elsevier Ltd.

### 1. Introduction

For cylinders with certain geometrical proportions, a buckling mode under wind loading exists which has not been extensively researched in the past. This buckling mode occurs for cylinders with radius-to-thickness ratios ( $R_0/t$ -ratios) and length-to-radius ratios ( $L/R_0$ -ratios) typically found for example in tall silos and is characterised by multiple ripple-like buckles in the area around the upper half of the windward meridian (termed the “front” of the cylinder in this paper). A recent case study for a cylinder displaying this type of buckling behaviour (Pircher, 2004) brought attention to the fact that this buckling mode is quite sensitive to the presence of axi-symmetric imperfections. In welded silos and tanks such imperfections are

\* Tel.: +61-2-47-360-307; fax: +61-2-47-360-833.

E-mail address: [m.pircher@uws.edu.au](mailto:m.pircher@uws.edu.au) (M. Pircher).

31 frequently present due to the building techniques employed for the erection of such structures. Steel plates  
 32 are typically bent into the required radius and then welded together horizontally and vertically to form the  
 33 final structure. The horizontal welds commonly span around the whole circumference of these silos and  
 34 inward-facing geometrical imperfections are typically found around these circumferential welds. The  
 35 geometry and other properties of these weld-induced circumferential imperfections have been discussed in  
 36 Pircher et al. (2000). The detrimental influence of axi-symmetric weld-induced imperfections on the  
 37 buckling behaviour of thin-walled cylinders under axial loading has been well documented in a number of  
 38 research papers (e.g., Steinhardt and Schulz, 1970; Rotter and Teng, 1989; Pircher and Bridge, 2001).  
 39 Greiner and Derler (1995) investigated the influence of a number of different imperfection shapes on the  
 40 buckling of silos under wind loading. However, axi-symmetric welds were not included in their study.

41 Depending on the geometry of a cylindrical structure three different stability failure modes can be ob-  
 42 served (Fig. 1). In low cylinders radial compression at the front of the cylinder causes tangential com-  
 43 pressive membrane forces  $N_\phi$  which result in a buckling mode similar to cylinders under radial compression  
 44 (mode 1 in Fig. 1). Very long cylinders display a distinctly different failure mode, whereby the compressive  
 45 axial forces  $N_x$  at the back of the cylinder trigger buckling in the lower third of the structure (mode 3 in Fig.  
 46 1) (e.g., Schneider and Zahlten, 2004). Mode 2 in Fig. 1 occurs for cylinders within a small range of  
 47 geometric parameters and is characterised by a number of ripple-like circumferential buckles in the upper  
 48 half of the meridian facing into the wind. The term “medium-length cylinders” in the context of this papers  
 49 refers to cylinders displaying this particular buckling mode under wind-loading. This mode was first  
 50 mentioned by Feder (1975) who reported on the failure of small PVC-specimens in a wind tunnel test with  
 51 additional axial loading. Greiner and Derler (1995) presented results of a numerical investigation of cyl-  
 52 inders under wind loading, some of which also displayed this failure characteristic. In this paper the  
 53 influence of axi-symmetric weld-induced imperfections on the buckling of a thin-walled cylinder displaying  
 54 this particular failure mode will be studied.

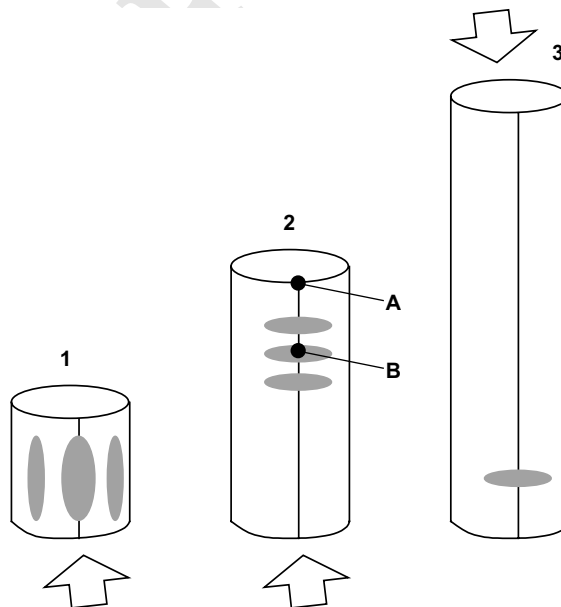


Fig. 1. Buckling of thin-walled cylinders under wind loading.

55 **2. Background**

56 *2.1. Structural model*

57 A thin-walled cylindrical shell with fixed bottom support and a diaphragm roof or rigid ring stiffener  
 58 restricting movement in the tangential and radial direction at the top was modelled using the finite elements  
 59 method. Fig. 2 captures the geometric properties  $R_0$ ,  $L$  and  $t$  of the described structural system and also  
 60 gives the naming conventions for the membrane stresses  $\sigma_x$ ,  $\sigma_\varphi$ ,  $\tau_{x\varphi}$  and displacements  $u$ ,  $v$  and  $w$ . The  
 61 geometry of the cylinder analysed for this case study is given by  $R_0 = 10$  m,  $R_0/t = 400$  and  $L/R_0 = 10$ .  
 62 Elastic material properties to resemble the behaviour of steel with a Young's modulus  $E = 2.1E8$  kN/m<sup>2</sup>  
 63 and a Poisson ratio of  $\nu = 0.3$  were defined. Since buckling was found to take place well in the elastic region  
 64 of the steel, no material non-linearities were taken into account. The computer model comprised half a  
 65 cylinder with planes of symmetry along the meridians facing into the wind ( $\varphi = 0$ ) and away from the wind  
 66 ( $\varphi = 180$ ).

67 *2.2. The failure mode*

68 The particular stability failure mode for medium-length cylinders which is the topic of this paper was  
 69 first mentioned in Feder (1975) and then again in Greiner and Derler (1995). A detailed case study of the  
 70 failure of a medium-length thin-walled cylinder under wind loading displaying this failure mode is given in  
 71 Pircher (2004). A cylinder with the same geometry as in this case study will be used for this paper. The  
 72 displaced shapes of a cylinder with no imperfections and with the same geometry as studied in this paper is  
 73 shown in Fig. 3 for various points along the load–displacement path under wind loading. A snap-through  
 74 failure mode into one large buckle covering a large area on the front side of the cylinder (long axial  
 75 wavelength mode) occurs first, closely followed by bifurcation into a failure mode with multiple horizontal  
 76 ripple-like buckles around two-thirds height of the cylinder (short axial wavelength mode). Two effects have  
 77 been found to contribute to the particular buckling behaviour of such cylinders: first, the presence of axial  
 78 compressive stresses in the upper half of the front-side of the cylinder and secondly, ovalisation of the cross-

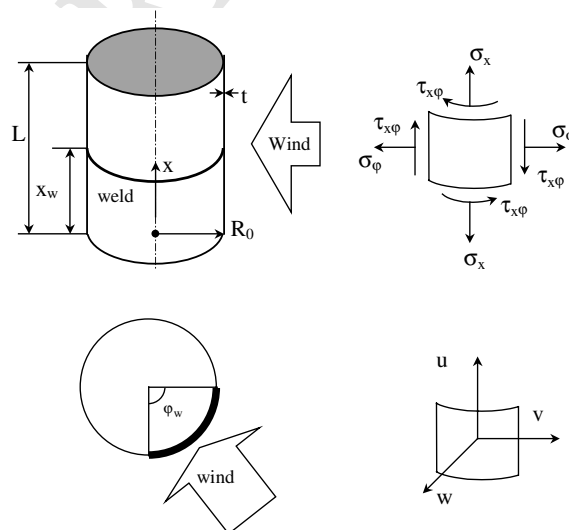


Fig. 2. Structural system, membrane stresses and displacements.

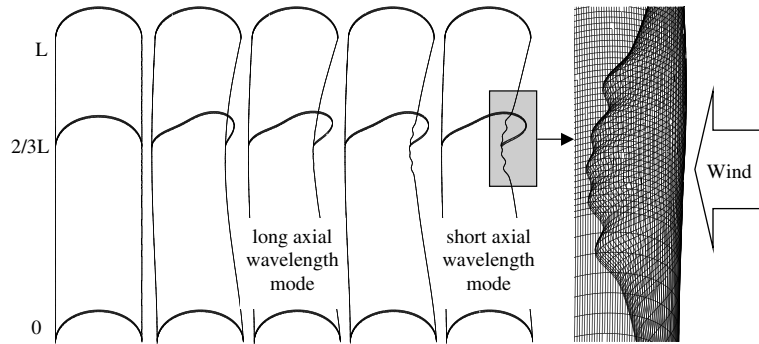


Fig. 3. Displaced shapes of the cylinder under wind loading at selected points along the load–displacement path.

79 section of the cylinder in areas away from the bottom and top supports. It was shown in Pircher (2004) that  
 80 the compressive axial forces trigger buckling which is aided by the decreased local resistance of the cylinder  
 81 due to the ovalised cross-section in this area. A supplementary eigenmode analysis found two closely spaced  
 82 bifurcation points which account for this buckling behaviour. Geometrically non-linear effects contribute  
 83 greatly to the buckling behaviour with a linear buckling analysis predicting an entirely different failure  
 84 mode. A brief imperfection sensitivity study in Pircher (2004) showed that for many different imperfection  
 85 shapes the structure was found to transform straight into the short axial wavelength mode without experi-  
 86 encing snap-through buckling into the long axial wavelength mode first.

### 87 2.3. Wind loading

88 A thorough discussion of many of the factors involved in wind pressure on circular cylindrical structures  
 89 can be found in Esslinger (1971), Kwok (1985) and Macdonald et al. (1988). The radial wind pressure varies  
 90 around the circumference and up the height of the cylinder. For this paper the governing radial component  
 91 of the wind loading around the circumference was assumed to be given by

$$p_{\text{Wind}}(\varphi) = \sum_{m=1}^n p_m \cos(m\varphi) = p_r \sum_{m=1}^n c_m \cos(m\varphi), \quad (1)$$

93 where  $p_r$  is the actual wind pressure onto the meridian facing the wind,  $c_m$  are the amplitudes of the Fourier  
 94 waves,  $m$  is the number of the individual Fourier waves and  $p_{\text{Wind}}(\varphi)$  is the resulting wind load. The material  
 95 developed for this paper uses values for  $c_m$  which have been suggested by Greiner and Derler (1995) with  
 96  $c_0 = -0.65$ ,  $c_1 = 0.37$ ,  $c_2 = 0.84$ ,  $c_3 = 0.54$ ,  $c_4 = -0.03$  and  $c_5 = -0.07$ . Wind pressure up the height of the  
 97 cylinder was assumed to be constant and the roof was not loaded. This structural system and model for  
 98 wind loading has been used in the past for investigations of thin-walled cylinders under wind loading (e.g.,  
 99 Greiner, 1983; Pircher et al., 2001b). For this paper all critical loads for imperfect structures  $p_{\text{cr,imp}}$  are given  
 100 in relation to the maximum load of the perfect structure which was found to be  $p_{\text{cr,perfect}} = 5.83 \text{ kN/m}^2$ . A  
 101 comparison of the stresses present at buckling under wind loading with the critical stresses for pure axial  
 102 and radial loading must take the significant ovalisation due to wind loading into account (Fig. 6). This  
 103 comparison along with a detailed explanation of the buckling mechanism of the geometrically perfect  
 104 system has been published in Pircher (2004). At this point it should be remarked that the displacements of  
 105 the loaded structure also have an influence on the wind loading pattern of the structure. This effect was not  
 106 taken into account for this investigation.

107 2.4. The axi-symmetric weld imperfection

108 Axisymmetric imperfections in circular cylindrical steel shell structures such as silos or tanks occur during  
109 construction when rolled steel plates are formed into a series of individual strakes and joined together by  
110 circumferential welds. The cooling of the welding material at the circumferential joints causes small inward  
111 deflections in the finished structure which are also accompanied by residual stresses. Pircher et al. (2001a)  
112 calibrated a theoretical approach based on elastic shell theory (Berry et al., 2000) against measured data  
113 and suggested a shape function given by

$$w(x) = A e^{-\pi x/\lambda} \left( \cos \frac{\pi x}{\lambda} + \zeta \sin \frac{\pi x}{\lambda} \right), \quad (2)$$

115 in which  $w(x)$  is the radial deviation from the perfect cylinder and  $A$  is the amplitude of the localised  
116 imperfection. The parameter  $\zeta$  defines the degree of roundness directly at the weld and is a measure for the  
117 variation of stiffness of the weld material during cooling of the weld. Parameter  $\lambda$  is the half-wavelength of  
118 the imperfection in the longitudinal direction which will be related to the linear meridional bending half-  
119 wavelength  $\lambda_0$  of a thin-walled cylinder given by

$$\lambda_0 = \pi \sqrt{\frac{R_0 t}{\sqrt{12(1 - \nu^2)}}} \approx 2.444 \sqrt{R_0 t}. \quad (3)$$

121 Other shape functions which have been suggested in the literature can be approximated by the given  
122 function by variation of the  $\zeta$  and  $\lambda$  parameters which is documented in Pircher et al. (2001a). In a number  
123 of papers (e.g., Rotter and Teng, 1989; Teng and Rotter, 1992; Pircher and Bridge, 2001; Song et al., 2004),  
124 the shape function given in Eq. (2) (or simplifications thereof) was used for an investigation of axisym-  
125 metrically imperfect cylinders under axial loading. The given function will be used again in this paper.

126 2.5. Imperfection sensitivity

127 A preliminary parametric study to investigate the imperfection sensitivity of the thin-walled cylinder  
128 under wind loading in this particular case study was performed in Pircher (2004). Several types of geometric  
129 imperfections were considered, among them eigenmode-affine shapes, a dent and axisymmetric shapes.  
130 Localised axisymmetric imperfections were found to be by far the most detrimental type of imperfection  
131 among the shapes tested in this paper. These results along with the fact that circumferential weld-induced  
132 imperfections have been shown to have an important influence on the buckling behaviour of thin-walled  
133 cylinders under axial loading led to the research results summarised in the present paper.

134 3. Results

135 3.1. Buckling and post-buckling behaviour

136 The buckling and the initial post-buckling behaviour changes due to the introduction of an axi-  
137 symmetric weld-like imperfection. Fig. 4(a) shows the front meridian of a perfect cylinder for selected  
138 points on the load–displacement curve for point B (Fig. 1). The load–displacement curve for this cylinder is  
139 shown in Fig. 4(b). The buckling behaviour with both stability failure modes as described above is clearly  
140 visible. The same diagrams for an axi-symmetric imperfection with  $\zeta = 0.5$  and  $\lambda/\lambda_0 = 2.0$  are shown in  
141 Fig. 5(a) and (b). Fig. 6 shows a horizontal cut through the cylinder at buckling for the perfect and the  
142 imperfect structure. The structure never displays the long axial wavelength mode but snaps straight into a

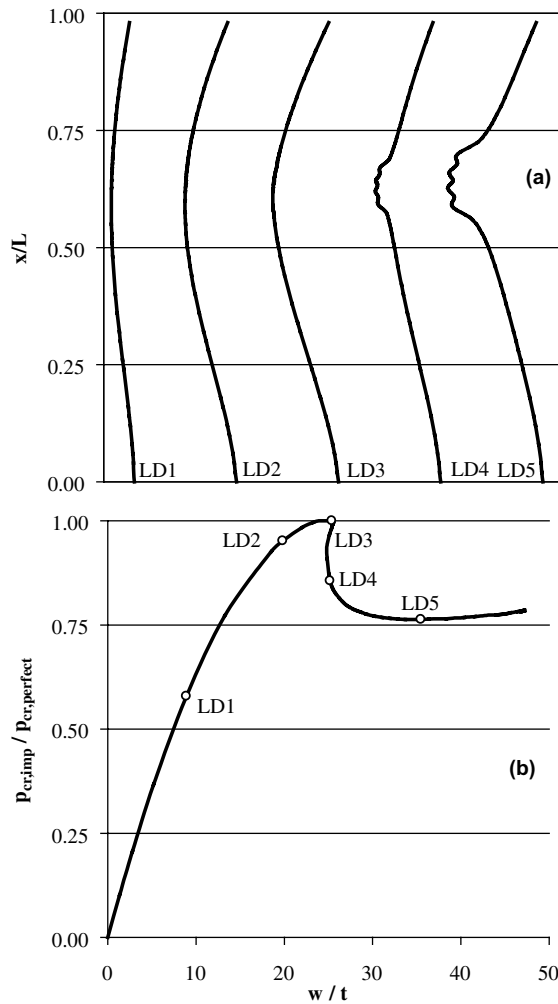


Fig. 4. Geometrically perfect model: front meridian (a) at selected points during load–displacement path (b).

143 buckling mode which is best characterised as a single horizontal fold-like buckle across the front of the  
 144 cylinder.

145 Various load–displacement characteristics (point B) for the same imperfection geometry ( $\xi = 0.5$  and  
 146  $\lambda/\lambda_0 = 2.0$ ), with various amplitudes ( $0 < A/t < 3.0$ ) are given in Fig. 7. For imperfection amplitudes up to  
 147 approximately  $A/t = 1.2$ , a clear local maximum load level can be observed after which the load-bearing  
 148 capacity drops off steeply before reaching a post-buckling minimum. After this minimum, in the presence of  
 149 considerable displacements, the wind load can be increased again. The post-buckling minimum is in a  
 150 similar place for all these load–displacement characteristics.

151 For cylinders with an axisymmetric imperfection with an amplitude  $A/t > 1.2$  no distinct maximum can  
 152 be defined in the load–displacement characteristics and no distinct point of stability loss could be observed  
 153 during the analysis. The transition from the “pre-buckling” section of the load–displacement curve into the  
 154 “post-buckling” section was found to be gradual. The imperfect structures were found to experience in-  
 155 creased deflection rates and the load–deflection path merged with the post-buckled load deflection path of

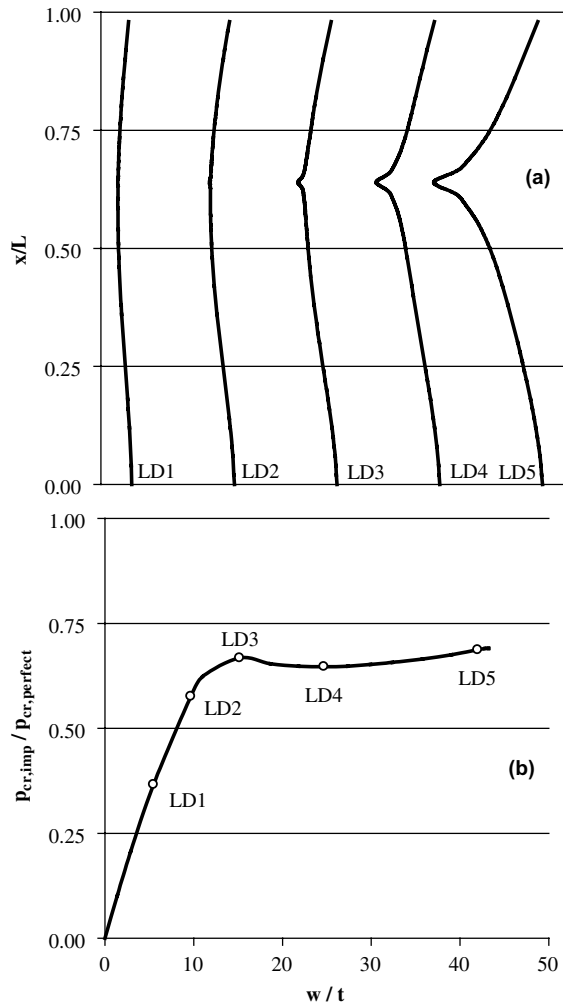


Fig. 5. Imperfect model ( $\xi = 0.5$ ,  $\lambda_i/\lambda_0 = 2.0$ ): front meridian (a) at selected points during load-displacement path (b).

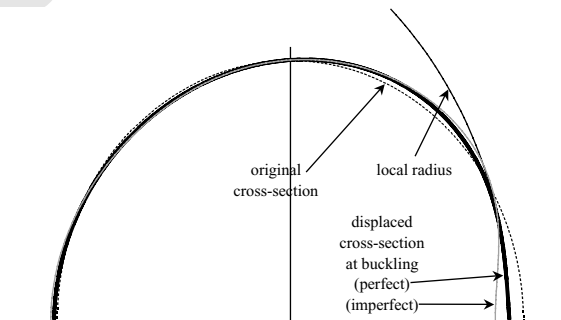


Fig. 6. Horizontal cut at weld height.

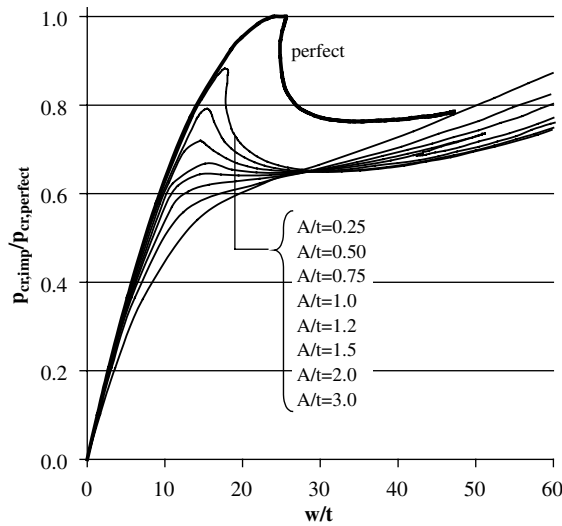


Fig. 7. Influence of axi-symmetric imperfections on the initial post-buckling behaviour.

156 the structures with smaller imperfection amplitudes  $A/t < 1.2$ . The load–displacement curves for all  
 157 imperfect FE models intersected at a point near the post-buckling minimum after which an increase in load  
 158 was possible beyond the initial maximum point. The displacements at this stage are large and an analysis  
 159 beyond this stage would have to consider displacement-dependent loading and also dynamic effects in order  
 160 to simulate wind loading conditions properly.

161 For the results presented in this paper geometrically non-linear analyses were performed. The critical  
 162 loads given in the following are local load maxima as explained above. For weld amplitudes  $A/t > 1.2$  no  
 163 such maxima can be defined. Since the typical weld imperfection found in silos usually does not exceed this  
 164 measure (Steinhardt and Schulz, 1970; Pircher et al., 2001a) it was found sufficient for the purpose of this  
 165 paper to limit the investigation to amplitudes  $A/t$  less or equal 1.2.

### 166 3.2. Weld position

167 In a first series of analyses the influence of the weld position  $x_w$  on the buckling resistance was inves-  
 168 tigated. The shape of the imperfection was set according to Eq. (2) with parameters  $\lambda/\lambda_0 = 1.0$  and  $\zeta = 0.5$ .  
 169 Fig. 8 illustrates this influence for various amplitudes of the imperfection. All graphs clearly show a  
 170 minimum of buckling resistance when the weld imperfection is situated at  $x_w/L = 0.64$ . For all further  
 171 analyses presented in this paper the axi-symmetric weld-like imperfection was placed at this position in the  
 172 finite element model.

### 173 3.3. Shape of the weld imperfection

174 Three non-dimensional parameters determine the shape of the axi-symmetric weld imperfection  
 175 according to Eq. (2): the amplitude  $A/t$ , the roundness parameter  $\zeta$  and the half-wavelength  $\lambda/\lambda_0$ . FE  
 176 models with imperfections of five different amplitudes ( $A/t = 0.25, 0.50, 0.75, 1.0, 1.2$ ) were built. For  
 177 each amplitude a diagram giving the buckling strength as a function of the half-wavelength was compiled  
 178 for three values of the roundness parameter  $\zeta$  ( $\zeta = 0.0, 0.5, 1.0$ ). The influence of these three parameters  
 179 on the buckling resistance is given in the five diagrams presented in Figs. 9–13. As can be seen in these

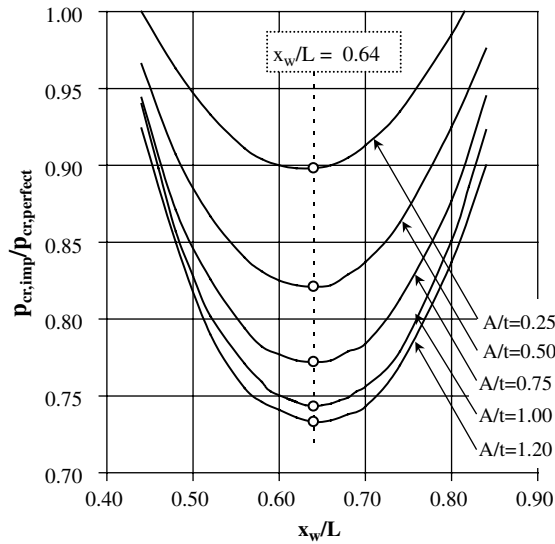


Fig. 8. Effect of weld position on the buckling strength.

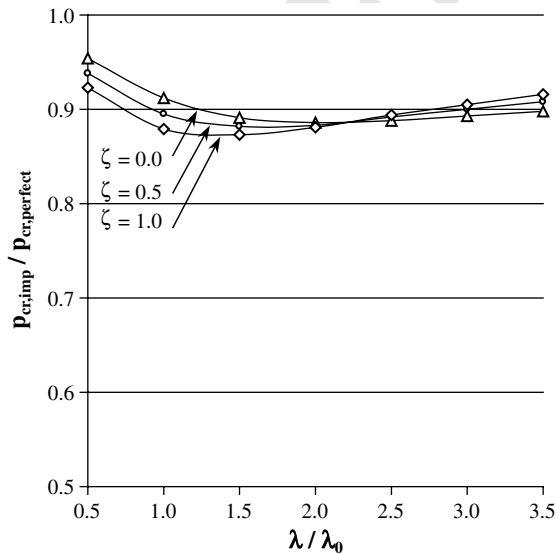


Fig. 9. Influence of the parameters  $\zeta$  and  $\lambda/\lambda_0$  on the buckling resistance for an imperfection amplitude  $A/t = 0.25$ .

180 diagrams, all three parameters influence the buckling resistance considerably. All diagrams show an  
 181 intersection point at  $\lambda/\lambda_i$  where the graphs for different values of  $\zeta$  intersect. For values of  $\lambda/\lambda_0 < \lambda_i/\lambda_0$   
 182 imperfections of  $\zeta = 1.0$  yield the lowest results for the buckling resistance, for values of  $\lambda/\lambda_0 > \lambda_i/\lambda_0$  welds  
 183 of  $\zeta = 0.0$  yield the lowest results. The position of this intersection point ( $\lambda_i/\lambda_0$ ) and also the position of the  
 184 minimum of buckling resistance ( $\lambda_{\min}/\lambda_0$ ) varies depending on the amplitude of the imperfection as shown  
 185 in Fig. 14. The decrease in buckling resistance as a function of the imperfection amplitude is shown in Fig.  
 186 15. The decrease in buckling strength under wind loading is considerable. For a weld imperfection with an

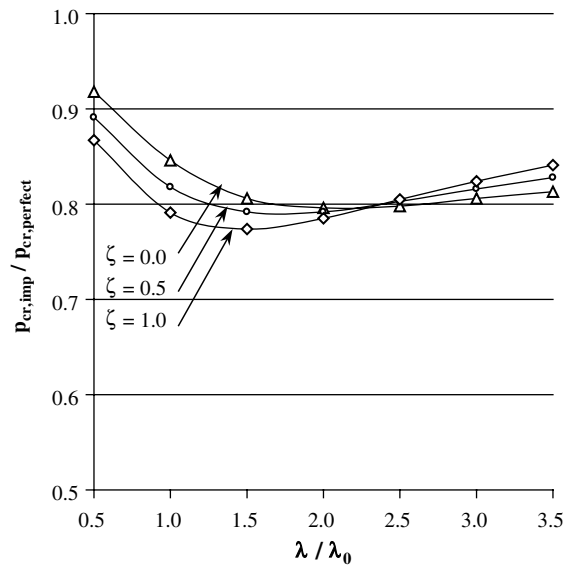


Fig. 10. Influence of the parameters  $\zeta$  and  $\lambda/\lambda_0$  on the buckling resistance for an imperfection amplitude  $A/t = 0.50$ .

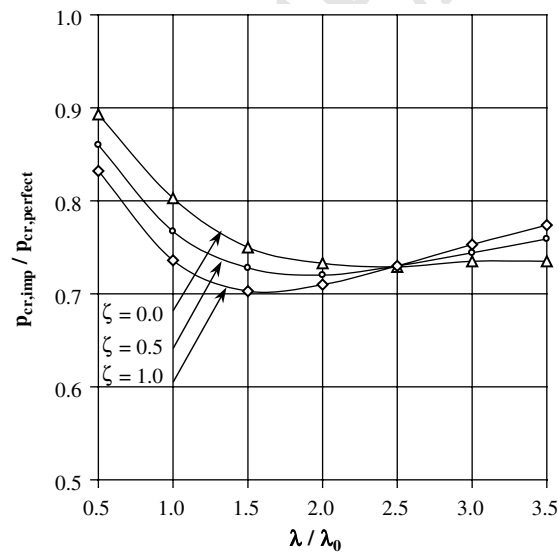


Fig. 11. Influence of the parameters  $\zeta$  and  $\lambda/\lambda_0$  on the buckling resistance for an imperfection amplitude  $A/t = 0.75$ .

187 amplitude of  $A/t > 1.0$  the buckling resistance is only 65% of the resistance of the nominally perfect cyl-  
188 inder.

189 3.4. Partial weld

190 In many cases circumferential welds in existing silos cause imperfections along significant portions of the  
191 circumference. Such an imperfection may be more severe in some places than in others. In order to

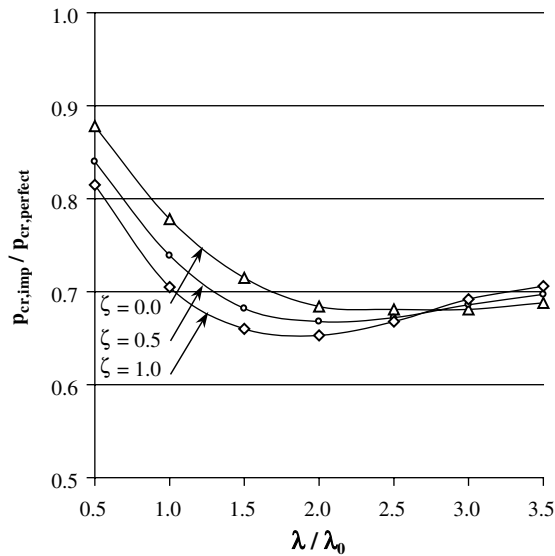


Fig. 12. Influence of the parameters  $\zeta$  and  $\lambda / \lambda_0$  on the buckling resistance for an imperfection amplitude  $A/t = 1.0$ .

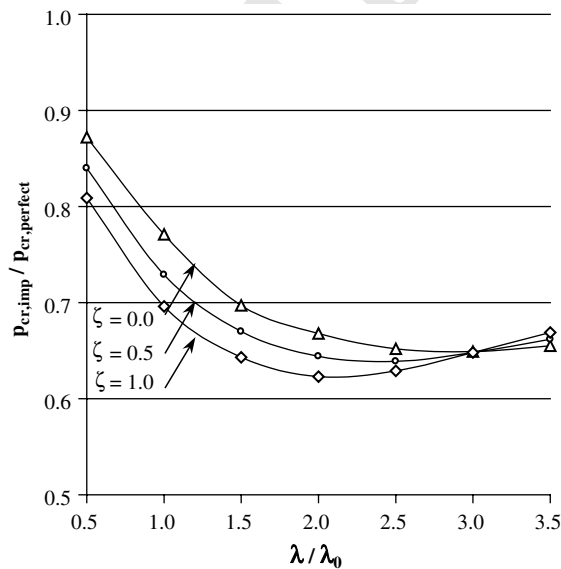


Fig. 13. Influence of the parameters  $\zeta$  and  $\lambda / \lambda_0$  on the buckling resistance for an imperfection amplitude  $A/t = 1.2$ .

192 investigate the influence of circumferential imperfections which span only across a part of the circumference  
193 ( $\varphi_w$ ), a series of analyses with partial weld imperfections was performed. Fig. 16 shows the buckling  
194 resistance for partial welds with an amplitude of  $A/t = 0.25$  for various shape parameters  $\lambda / \lambda_0$  and  $\zeta$ . A  
195 minimum in buckling resistance can be observed at  $\varphi_w = 20^\circ$ . Shortly after this minimum the graph for the

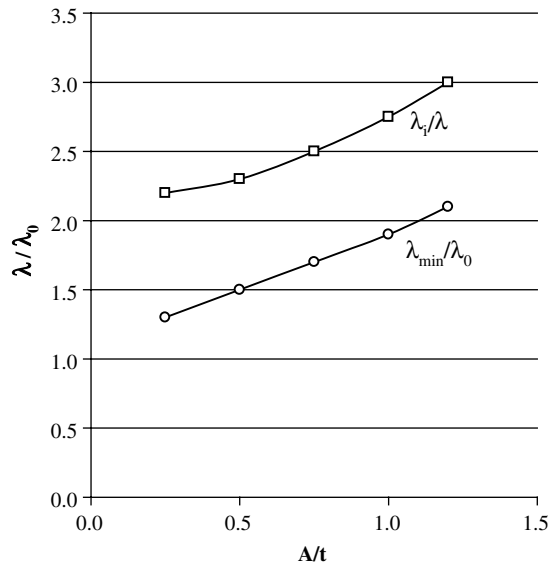


Fig. 14. Position of the intersection point for various  $\zeta(\lambda_i/l_0)$  and the minimum for the buckling resistance ( $\lambda_{\min}/l_0$ ).

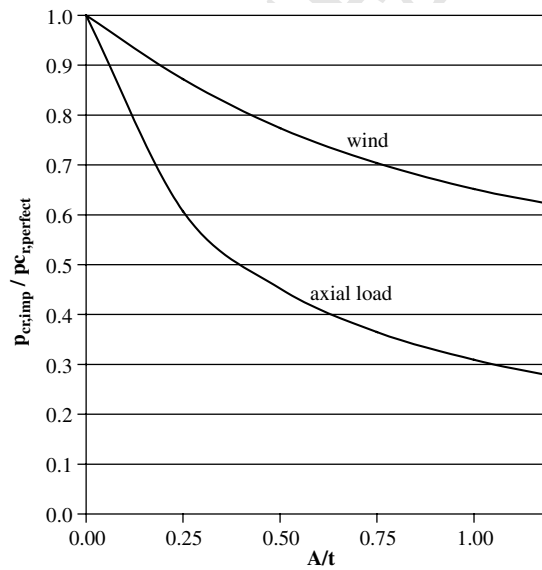


Fig. 15. Influence of imperfection amplitude on the buckling resistance.

196 buckling resistance levels out at a value equal to the value for a full circumferential weld. A similar  
 197 behaviour was observed for other imperfection amplitudes. Consequently, it can be stated that a weld  
 198 imperfection which spans only over 20° of the circumference must be viewed as equally detrimental as a full  
 199 circumferential weld imperfection for cylinders under wind loading.

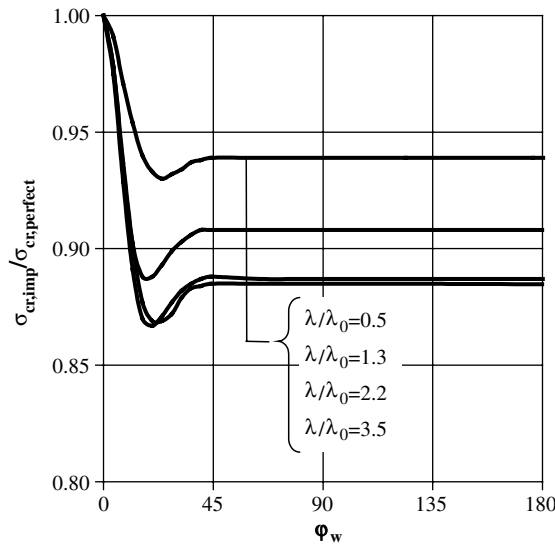


Fig. 16. Partial weld, amplitude  $A/t = 0.25$ .

200 3.5. Residual stresses

201 Shrinkage of the weld material not only introduces a geometrical imperfection into a cylindrical shell  
 202 structure but also creates a residual stress field in the vicinity of the weld. Circumferential tension stresses at  
 203 the weld often reach yield level and are typically balanced by significant compression stresses further away  
 204 from the weld. The welding process creating this residual stress field can be approximated by applying  
 205 appropriate strain loading at the weld. This method was first proposed by Rotter (1996) and was also used  
 206 for this study. Comparing geometrically equal models with and without residual stress field showed that in  
 207 the case of wind loading the buckling resistance was reduced due to residual stresses. However, for all  
 208 considered cases this reduction was less than 2%.

209 3.6. Comparison with axial compression

210 The buckling behaviour of thin-walled cylinders with a weld imperfection in axial compression has been  
 211 researched extensively. A comparison with the findings described in this paper for the wind loading case will  
 212 be given in the following. Eq. (4) gives the classical buckling strength  $\sigma_{\text{cl}}$  of thin-walled cylinders in axial  
 213 compression which will be used as a reference value for axial compression:

$$\sigma_{\text{cl}} = \frac{Et}{R\sqrt{3(1-\nu^2)}} \approx 0.605 \frac{Et}{R}. \quad (4)$$

215 Teng and Rotter (1992) used a simplified shape function related to Eq. (2) in this paper and showed that  
 216 the buckling resistance varied for  $\zeta = 0.0$  and  $1.0$  for the same imperfection amplitude. Pircher and Bridge  
 217 (2001) varied all three shape parameters ( $A/t$ ,  $\lambda/\lambda_0$  and  $\zeta$ ) of the shape function for imperfect cylinders and  
 218 determined the influence of the weld shape on the buckling behaviour. Qualitatively this influence is very  
 219 similar for both loading cases. The diagrams for axial compression given in Pircher and Bridge (2001) very  
 220 much resemble the diagrams given in this paper in Figs. 9–13. For both loading cases the weld imperfection  
 221 has been shown to lead to severe reductions in buckling resistance—significantly surpassing the influence of

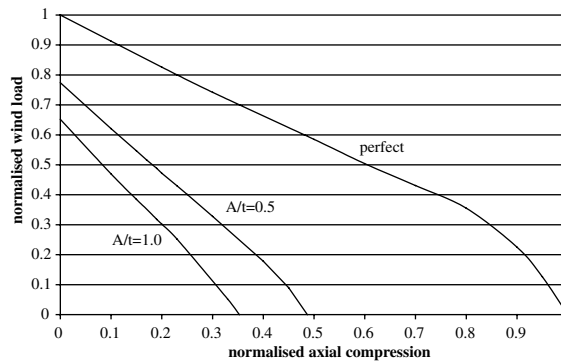


Fig. 17. Interaction diagram—axial compression and wind loading.

222 other imperfection shapes. The reduction of buckling resistance for various imperfection amplitudes for  
 223 both loading cases can be seen in Fig. 15, where  $p_{cr,perfect}$  refers to  $\sigma_{cl}$  as given in Eq. (4) for the axial loading  
 224 case. While the position of the weld matters under wind loading, this is not the case for cylinders under axial  
 225 compression (as long as the weld is positioned far enough away from the end constraints). Berry (1997)  
 226 briefly investigated the effect of partial welds on the buckling behaviour under axial loading and found a  
 227 similar behaviour as described in this paper for the wind loading case. Weld-induced residual stresses in-  
 228 crease the buckling strength of cylindrical shell structures under axial loading by a small amount (Rotter,  
 229 1996; Pircher and Bridge, 2001) but decrease the buckling resistance of these structures under wind loading,  
 230 again by a very small amount.

### 231 3.7. Interaction between wind loading and axial compression

232 Since axial compression and wind loading often occur simultaneously the interaction between the two  
 233 loading cases was investigated. For the present study axial compression was applied onto the cylinder in a  
 234 first step and wind loading was then applied and increased incrementally until stability failure occurred.  
 235 Axial loading will be given normalised against  $\sigma_{cl}$ . Fig. 17 shows the interaction diagram for buckling under  
 236 a combination of the two loading conditions for three different imperfection amplitudes  
 237 ( $A/t = 0.0, 0.5$  and  $1.0$ ). For the nominally perfect models the interaction diagram is slightly non-linear  
 238 for cases with a high level of axial compression. For cylinders with weld imperfections the relationship is  
 239 very close to linear.

## 240 4. Conclusions

241 A case study for a thin-walled cylindrical shell structure under wind loading has been presented. The  
 242 geometric parameters of the cylinder were chosen so that a particular buckling pattern occurred. This  
 243 pattern is characterised by horizontal ripple-like buckles in the upper half of the side of the cylinder facing  
 244 the wind. In this area considerable axial compression occurs. Two critical factors trigger this type of sta-  
 245 bility failure: first, the ovalisation at the critical cross-section and secondly the disproportional increase of  
 246 axial compression due to geometrically non-linear effects. Axi-symmetric weld imperfections were shown to  
 247 reduce the buckling resistance of such a thin-walled cylinder considerably. An investigation into the nature  
 248 of this influence has yielded the following results:

- The position of the weld along the height of the thin-walled cylinder has a great influence on the buckling strength under wind-loading. A weld positioned at 0.64 times the height of the cylinder leads to the greatest reduction in buckling strength.
- The shape of the weld imperfection can be described by three parameters: the “roundness”, the half-wavelength and the amplitude. All three parameters influence the extent of the reduction.
- A partial weld spanning only 20° of the circumference already has the same effect as a full 360° weld imperfection.
- Weld-induced residual stress fields reduce the buckling resistance by a small amount.
- Strong similarities exist with the influence of such an imperfection on the buckling behaviour under axial compression. Interaction diagrams are given for the two loading conditions revealing an interaction characteristic which is close to linear.

## Acknowledgements

The author thank Prof. R. Greiner and Prof. W. Guggenberger from the Institut für Stahlbau, Holzbau und Flächentragwerke at the Graz University of Technology in Austria and Prof. R.Q. Bridge from the Centre for Construction Technology and Research, University of Western Sydney in Australia for their support and their input into the work leading to this paper.

## References

- Berry, P.A., 1997. Buckling under axial compression of cylindrical shells with circumferential weld shrinkage depressions. PhD thesis, University of Sydney.
- Berry, P.A., Rotter, J.M., Bridge, R.Q., 2000. Compression tests on cylinders with circumferential weld depressions. *ASCE Journal of Engineering Mechanics* 126 (4), 405–413.
- Esslinger, M., 1971. Stationäre Windbelastung offener und geschlossener kreiszylindrischer Silos. *Der Stahlbau* 12, 361–368 (in German).
- Feder, G., 1975. Einige qualitative Bemerkungen zum Beulen von stehenden Behältern unter Windlast. In: Esslinger, M., Geier, B. (Eds.), *Sonderheft der Deutschen Forschungs- und Versuchsanstalt für Luft- und Raumfahrt, Braunschweig* (in German).
- Greiner, R., 1983. Zur ingenieurmässigen Berechnung und Konstruktion zylindrischer Behälter aus Stahl unter allgemeiner Belastung. *Wissenschaft und Praxis, Band 31, Fachhochschule Biberach, Germany* (in German).
- Greiner, R., Derler, P., 1995. Effect of imperfections on wind-loaded cylindrical shells. *Thin-Walled Structures* 23, 271–281.
- Kwok, K.C.S., 1985. Wind loads on circular storage bins. In: *Proceedings: Joint US–Australian Workshop on Loading, Analysis and Stability of Thin Shell Bins, Tanks and Silos, University of Sydney*, pp 49–54.
- Macdonald, P.A., Kwok, K.C.S., Holmes, J.D., 1988. Wind loads on circular storage bins, silos and tanks: I. Point pressure measurements on isolated structures. *Journal of Wind Engineering and Industrial Aerodynamics* 31 (2–3), 165–188.
- Pircher, M., 2004. Medium-length thin-walled cylinder under wind loading—a case study. *Journal of Structural Engineering, ASCE* (submitted for publication).
- Pircher, M., Berry, P.A., Bridge, R.Q., 2000. The properties of circumferential weld-induced imperfections in silos and tanks. *Engineering Report CE17, School of Engineering & Industrial Design, University of Western Sydney*.
- Pircher, M., Bridge, R.Q., 2001. Buckling of thin-walled silos and tanks under axial load some new aspects. *Journal of Structural Engineering, ASCE* 127 (10), 1129–1136.
- Pircher, M., Berry, P.A., Ding, X., Bridge, R.Q., 2001a. The shape of circumferential weld-induced imperfections in thin-walled steel silos and tanks. *Thin-Walled Structures* 39 (12), 999–1014.
- Pircher, M., Guggenberger, W., Greiner, R., 2001b. Stresses in elastically supported cylindrical shells under wind load and foundation settlement. *Advances in Structural Engineering* 4 (3), 159–167.
- Rotter, J.M., Teng, J.G., 1989. Elastic stability of cylindrical shells with weld depressions. *Journal of Structural Engineering, ASCE* 115 (5), 1244–1263.
- Rotter, J.M., 1996. Buckling and collapse in internally pressurised axially compressed silo cylinders with measured axisymmetric imperfections: imperfections, residual stresses and local collapse. In: *Imperfections in Metal Silos Workshop, Lyon, France*, pp 119–139.

- 296 Schneider, W., Zahlten, W., 2004. Load-bearing behaviour and structural analysis of slender ring-stiffened cylindrical shells under  
297 quasi-static wind load. *Journal of Constructional Steel Research* 60, 125–146.
- 298 Song, C.Y., Teng, J.G., Rotter, J.M., 2004. Imperfection sensitivity of thin elastic cylindrical shells subject to partial axial compression.  
299 *International Journal of Solids and Structures* (in press).
- 300 Steinhardt, O., Schulz, U., 1970. Zur Beulstabilität von Kreiszyklinderschalen. Bericht der Versuchsanstalt fuer Stahl, Holz, Steine,  
301 Universitaet Karlsruhe (in German).
- 302 Teng, J.G., Rotter, J.M., 1992. Buckling of pressurised axisymmetrically imperfect cylinders under axial loads. *Journal of Engineering*  
303 *Mechanics*, ASCE 118 (2), 229–247.

UNCORRECTED PROOF